INVESTIGATION OF A DUAL RESONANT CAVITY ABSORPTION CELL USING THE DOUBLE-RESONANCE MICROWAVE SPECTROSCOPY MODULATION TECHNIQUE

A Thesis

Presented to

the Faculty of the School of Engineering and Applied Science

University of Virginia

In Partial Fulfillment

of the Requirements for the Degree

Master of Electrical Engineering

---

by

Major Clinton Lee

August 1968

APPROVAL SHEET

This thesis is submitted in partial fulfillment of

the requirements for the degree of

Master of Electrical Engineering

_____

Author

Approved:

_____

Faculty Advisor

_____

Dean, School of Engineering
and Applied Science

August 1968

ACKNOWLEDGMENTS

The author wishes to acknowledge Dr. H. S. Landes of the University of Virginia for his helpful suggestions in the preparation of this thesis, Mr. W. F. White, and the NASA-Langley Research Center for making it possible for this work to be submitted as a thesis.

TABLE OF CONTENTS

CHAPTER		PAGE
I.	INTRODUCTION	1
II.	DOUBLE-RESONANCE AND INTERFEROMETER THEORY	4
III.	THE EXPERIMENTAL SYSTEM	9
IV.	RESULTS	12
V.	CONCLUSIONS	23
	Sensitivity Factors	23
	Sample Properties	23
	Frequency Capability	24
REFERENCES		25
APPENDICES		
APPENDIX I		26

LIST OF TABLES

TABLE PAGE

I. Interferometer Parameters for the Various Conditions . . . 13

LIST OF FIGURES

FIGURE PAGE

1. Block diagram of a double-resonance modulated microwave spectrometer 2
2. One possible energy level scheme for which a double-resonance effect can be expected to occur 5
3. Double-resonance spectrometer utilizing the dual resonant cavity absorption cell 10
4. Sample strip chart recording of the $0_{00} \rightarrow 1_{11}$, $1_{11} \leftarrow 2_{02}$ double resonance of methylene chloride with the modulated pump signal being slowly swept across 15,911.9 MH_z 14
5. Signal amplitude variations for the $0_{00} \rightarrow 1_{11}$, $1_{11} \leftarrow 2_{02}$ double resonance of methylene chloride at 100 microns pressure 15
6. Noise amplitude plot for the observing circuit 18
7. Signal-to-noise ratio variation of the $0_{00} \rightarrow 1_{11}$, $1_{11} \leftarrow 2_{02}$, double resonance of methylene chloride at 100 microns pressure with $Q_p = 16,000$ and $Q_o = 59,250$ 19
8. Signal amplitude variations for the $0_{00} \rightarrow 1_{11}$, $1_{11} \leftarrow 2_{02}$, double resonance of methylene chloride at 25 microns pressure and different levels of pump cavity excitation power 20

FIGURE PAGE

9. Signal amplitude variations for the $0_{00} \rightarrow 1_{11}$, $1_{11} \leftarrow 2_{02}$, double resonance of methylene chloride at 100 microns pressure and different levels of pump cavity excitation power 21

10. Signal amplitude variations for the $0_{00} \rightarrow 1_{11}$, $1_{11} \leftarrow 2_{02}$, double resonance of methylene chloride at 150 microns pressure and different levels of pump cavity excitation power. 22

11. Confocal interferometer configuration 27

12. Semiconfocal interferometer configuration 29

LIST OF SYMBOLS

a.m.	amplitude modulation
A_o	effective area of cavity input transmission line
A_r	effective area of cavity
b	curved mirror radius of curvature
C	constant
d	reflector separation not equal to radius of curvature of curved mirror
dB	decibel
E	microwave radiation field
f	frequency
f.m.	frequency modulation
K	gas saturation coefficient
KH_z	kilohertz (10^3 cycles per second)
L	reflector separation
L_{eff}	effective path length
m	number of field reversals in a direction transverse to the interferometer axis of symmetry
MH_z	megahertz (10^6 cycles per second)
mW	milliwatt (10^{-3} watts)
n	number of field reversals in a transverse direction orthogonal to the direction assumed for m
P	power
Q	cavity quality factor

q	integral number of half wavelengths between reflectors
RF	radio frequency
V_D	detected signal voltage
α	absorption coefficient
α_t	total transit losses
ΔE	microwave field change
η	molecular density function
ϕ	intensity function
λ	wavelength

ABSTRACT

The application of a dual resonant cavity absorption cell composed of two Fabry-Perot interferometers mounted at right angles in a suitable vacuum enclosure to observe the double resonance effect is investigated. Each interferometer is excited by an independent microwave source. The double-resonance transition is modulated by one source and the modulation induced on the RF absorption in the orthogonal cavity detected. Experimental data are presented to show signal amplitude variations for the two connected transitions of methylene chloride, $0_{00} \rightarrow 1_{11} = 35{,}067.0\ MH_z$ and $1_{11} \leftarrow 2_{02} = 15{,}911.9\ MH_z$, as sample pressure, microwave power levels, and cavity Q's were varied. Sensitivities obtained are comparable to those of conventional Stark modulated microwave spectrometers and further improvements are anticipated as higher frequencies are studied.

CHAPTER I

INTRODUCTION

If microwave energy is propagated through a polar gaseous sample, absorption of the power will occur at frequencies characteristic of the separation of the molecular rotation energy levels. Absorption frequencies are characteristic of the molecular structure.

The sensitivity of the absorption detection is enhanced in the Stark modulated spectrometer by the introduction of an alternating electric field applied transverse to the direction of propagation of the microwave power. The perturbation of the gas molecules due to the applied electric field is called the Stark effect and results in a modulation of the amount of power absorbed by the gas. Utilizing the applied electric field modulation, cross-correlation detection techniques can be used to obtain greatly increased signal-to-noise ratios over direct absorption detection (Ref. 1, p. 1).

For a mixture possessing a rich microwave spectra, Stark modulation can cause interference from neighboring and/or overlapping lines. Microwave double-resonance spectroscopy allows a selective modulation of energy transitions and eliminates the interference problem. It affords an extremely precise method for identifying individual components of a mixture with only one observed double resonance needed for each identification (Ref. 1, p. 1).

Research Systems Incorporated has developed the double-resonance spectrometer shown in block form in Figure 1 (Ref. 1, pp. 28-33).

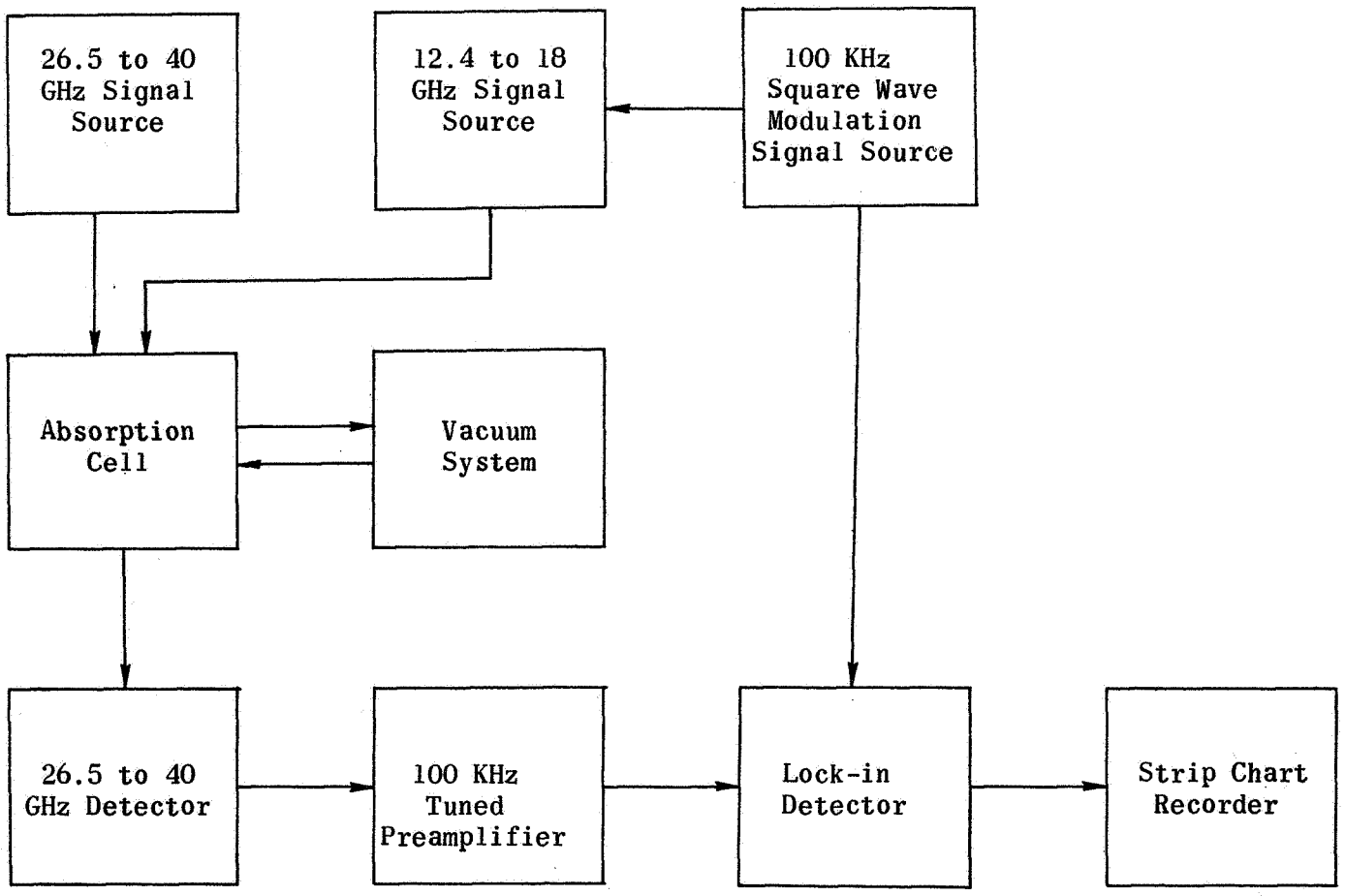

Figure 1.- Block diagram of a double resonance modulated microwave spectrometer.

This instrument utilized an absorption cell consisting of 100 feet of copper X-band waveguide coiled to reduce space requirements. The two major difficulties encountered in the use of this type cell are its poor vacuum and microwave characteristics. In an effort to improve on these two characteristics, a cell was designed which utilizes two orthogonal Fabry-Perot interferometers to irradiate a gaseous sample with two different microwave signals. This thesis presents results obtained by use of the Fabry-Perot dual resonant cavity design for the detection of the $0_{00} \rightarrow 1_{11}$, $1_{11} \leftarrow 2_{02}$* double-resonance effect of the methylene chloride molecule. This methylene chloride double-resonance effect was selected for evaluation of the absorption cell because it is typical of the transitions in the microwave frequency range.

*See Reference 2, Chapter 4, for a discussion of this type energy level designation.

CHAPTER II

DOUBLE-RESONANCE AND INTERFEROMETER THEORY

If a gaseous sample is irradiated by two microwave signals of frequencies f_1 and f_2, each corresponding to an allowed molecular energy transition, two photon exchanges by a single molecule can occur if certain conditions are met. First, the two transitions must have one energy state in common. Second, the intensity of one or both fields must be high enough to produce appreciable power saturation. Figure 2 shows one possible arrangement of the three quantum states (Ref. 3, p. 928).

The two radiation fields utilized can be defined as

$$E_2 = E_{02} \cos 2\pi f_2 t \tag{1}$$

$$E_1 = E_{01} \cos 2\pi f_1 t \tag{2}$$

The field E_2 will be called the observing field and the field E_1 the pump field. If the microwave energy field E_1 irradiates a gaseous sample and is turned on and off in a square wave manner then the density of molecules having energy levels 1 and 2 will be modulated. This modulation of energy level densities will cause small but readily detectable changes in the intensity of the absorption of radiation from the second field E_2 if E_1 and E_2 are irradiating the same gaseous sample. The detected signal consists only of changes in power absorption of the field E_2.

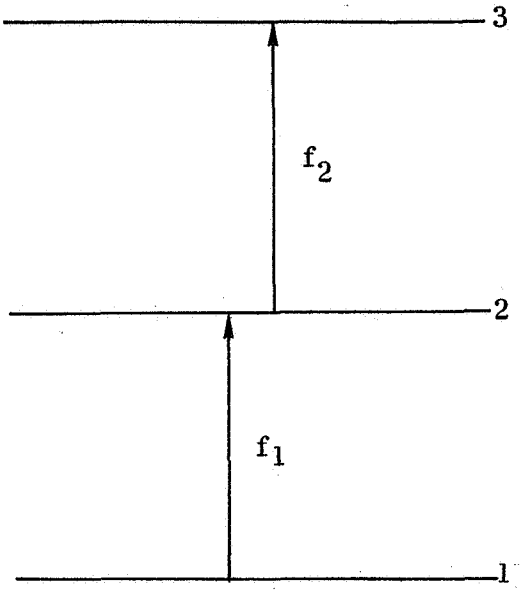

Figure 2.- One possible energy level scheme for which a double resonance effect can be expected to occur.

Microwave double-resonance spectroscopy has, until this work, been performed only in waveguide absorption cells. These cells consist of a section of oversize waveguide in which to confine the gaseous sample of interest. To obtain high sensitivities and reduce space requirements, long sections of waveguide were coiled and used as the absorption cell. In an effort to place the gaseous sample in a more favorable environment to interact with the radiating fields, an absorption cell was designed to apply characteristics of the Fabry-Perot interferometer to double-resonance spectroscopy.

The microwave version of the Fabry-Perot interferometer* has been used to observe single energy transition effects by several authors as reported in the literature (Refs. 4, 5, 6, and 7). Their results indicate that if an absorption modulation technique were used, such as double resonance, then comparatively high sensitivities might be obtained.

The Q of a resonant cavity is given by

$$Q = \frac{f_o}{\Delta f} \tag{3}$$

where f_o is the center frequency of the cavity response and Δf is the half-power bandwidth of the cavity response. A Fabry-Perot resonator absorption cell has an effective path length which is related to its Q by (Ref. 7, p. 590)

$$L_{eff} = \frac{Q\lambda}{2\pi} \tag{4}$$

---

*See Appendix I for a discussion of the confocal and semiconfocal microwave Fabry-Perot interferometer.

For a $Q = 60{,}000$ and a frequency of $35{,}000\ MH_z$, $L_{eff} = 269$ feet. This shows the obvious advantage of using a Fabry-Perot resonator for low loss measurements. Also,

$$Q = \frac{2\pi L}{\lambda \alpha_t} \tag{5}$$

where α_t are the total losses per transit and L is the mirror spacing (Ref. 4, p. 1,604). Hence,

$$\frac{L_{eff}}{L} = \frac{1}{\alpha_t} \tag{6}$$

Cavity losses therefore determine the "improvement factor" $\left(\frac{L_{eff}}{L}\right)$. These losses are about 0.1 percent or less per reflection for the mirror materials used (Ref. 4, p. 1,604). The other losses are due to diffraction, coupling to the cavity, and gas absorption. Diffraction losses are made negligible by the use of a semiconfocal configuration (Ref. 4, p. 1,604). A larger source of loss results in coupling energy to the resonator. The commonly used method of exciting semiconfocal cavities uses direct waveguide coupling through a small iris near the center of the flat mirror. This type of coupling usually results in a coupling loss of a few tenths percent (Ref. 4, p. 1,604). A disadvantage of this method is the difficulty encountered in changing the Q.

When a lossy gas is introduced into a resonator, its frequency response changes and the Q decreases. The absorption (α) of the gas is given by (Ref. 4, p. 1,605)

$$\alpha = \left(\frac{2\pi}{\lambda Q_l}\right)\left[\left(\frac{Q_l}{Q_g}\right) - 1\right] \text{cm}^{-1} \qquad (7)$$

Q_l and Q_g are the cavity quality factors without and with the gas, respectively.

CHAPTER III

THE EXPERIMENTAL SYSTEM

A block diagram of the spectrometer system including the dual resonant cavity absorption cell is shown in Figure 3. The interior for the absorption cell is in the form of a cube approximately 10 × 10 × 10 inches. Its walls are made of 1/2-inch-thick stainless steel with the joints welded. Holes are cut and O-ring seals used for the mounting of the flat mirrors and linear motion feedthrough supports for the curved mirrors. Vacuum connections for pumpdown and sample inlet to the cell are made through two sections of 1/2-inch o.d. stainless steel tubing welded into the chamber walls. The flat and curved mirrors are machined out of brass and gold plated for improved reflectivity and vacuum characteristics. The mirrors protrude into the chamber in such a way that wall reflections which might result in unwanted resonances will be reduced.

The curved mirrors are 6 inches in diameter and have a radius of curvature of 14 inches. The flat mirrors are also 6 inches in diameter. Two separate irises are soldered onto the ends of the waveguides and the irises are mounted as part of the flat mirror face for coupling microwave energy into and out of each cavity. Mica window vacuum seals are mounted onto the flange end of the waveguides. The interferometers are arranged so that the microwave fields propagate at right angles, but with their electric field vectors parallel. The distance from the flat mirror to the curved mirror of each interferometer is 7 $\pm$1/2 inches.

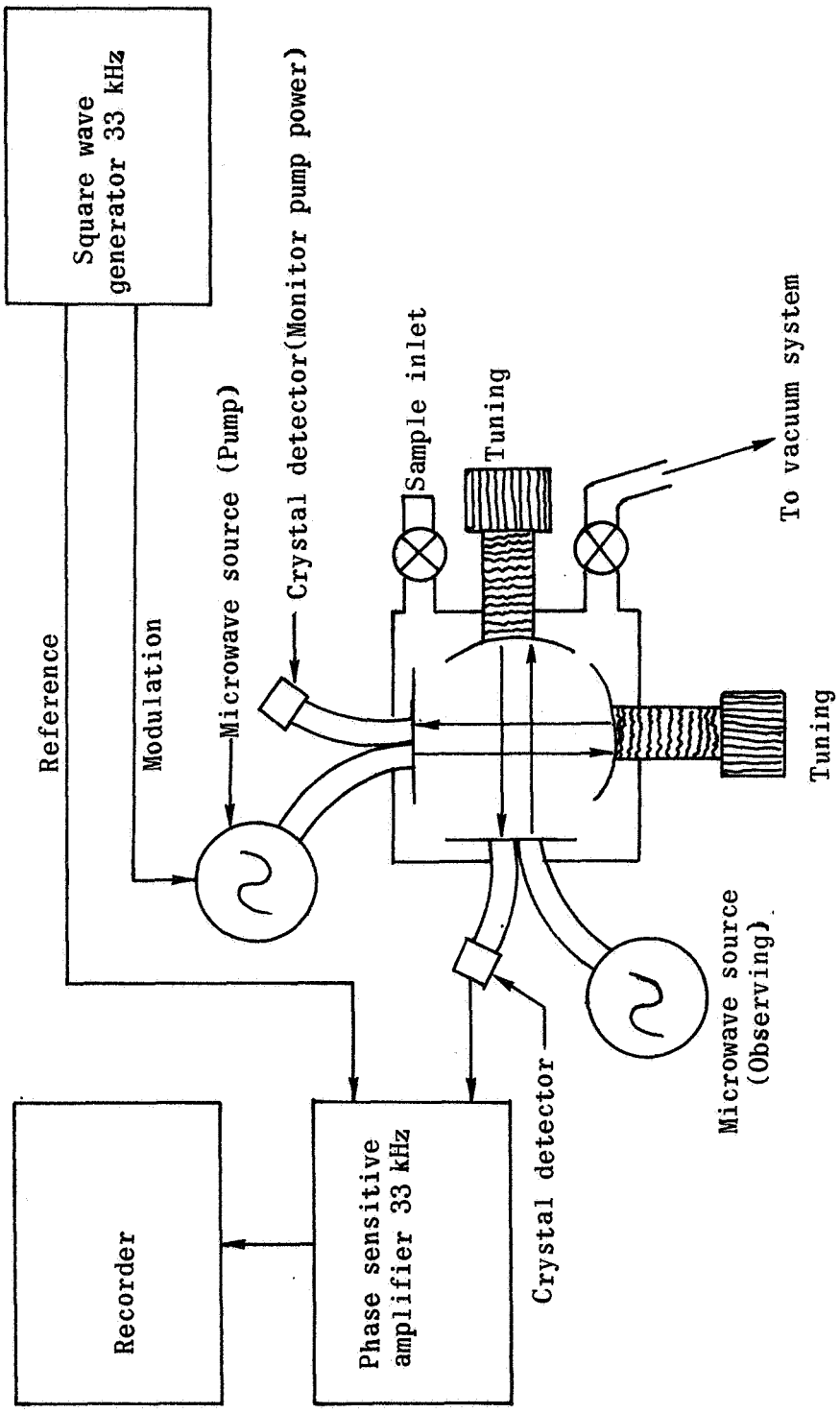

Figure 3.- Double resonance spectrometer utilizing the dual resonant cavity absorption cell.

The ±1/2 inch is the travel allowed by the linear motion feedthroughs for tuning the interferometers to the desired resonant frequencies.

Variation of the Q's of the two cavities was accomplished by varying the size of one of the irises of each of the flat mirrors. The Q's were determined by measuring the free space values of f_o and Δf for both cavities and substituting these values into equation (3). The presence or absence of the field of one cavity does not affect the Q of the other cavity for the free space case. As previously stated, the introduction of a lossy gas into a resonant cavity decreases its Q. This decrease was so small for this experimentation that no attempt was made to measure it directly.

The first step in the operation of the absorption cell was to tune each of the cavities to the required frequency. For the case of the selected methylene chloride double-resonance effect, the frequencies are 15,911.9 MH_z for the pumping cavity and 35,067.0 MH_z for the observing cavity. In order to produce a strip chart recording of the double-resonance effect, the observing source was phase locked to a very stable reference and the modulated pump source was swept through its cavity resonance.

Because of equipment limitations, direct amplitude modulation of the pump source was not possible. An alternate method selected used high deviation square wave f.m. of the pump source. The resulting on-off nature of the power inside the pump cavity was essentially that of an amplitude modulated signal.

CHAPTER IV

RESULTS

Table I lists the various cavity parameters utilized in this experimentation. Changes in the iris diameters were made by standard size drill bits. The cavities were tuned to the desired f_o and the half-power bandwidth, Δf, measured for each. The values obtained were substituted into equation (3) to obtain the Q's.

An example of the strip chart recordings of the lock-in detector output indicating the methylene chloride double-resonance effect is shown in Figure 4. Pump frequency is the abscissa and the output of the lock-in detector, which is proportional to the observed power variation in phase with the modulation on the pump signal, is the ordinate.

The set of curves given in Figure 5 is the maximum signal cases for the five different combinations of cavity Q's utilized in observing the $0_{00} \rightarrow 1_{11}$, $1_{11} \leftarrow 2_{02}$ methylene chloride double resonance. For these cases, the maximum available pump cavity exciting power was utilized to obtain the signal amplitude versus observing detector power plots. A sample pressure of 100 microns and maximum available pump cavity exciting power were found to produce maximum signal from the methylene chloride molecular double resonance for any combination of the resonant cavity parameters.

In order to reduce the ratio of cavity power to detector power for the observing cavity the iris coupling to the observing detector was enlarged (see Table I). This resulted in a given amount of exciting

TABLE I.- INTERFEROMETER PARAMETERS FOR THE VARIOUS CONDITIONS

Pump cavity at 15,911.9 MH_z			
Inlet iris diameter (in.)	Outlet iris diameter (in.)	Q	Insertion loss (dB)
0.1285	0.1285	21,000	19.5
0.136	0.1285	16,000	17.5
Observing cavity at 35,067.0 MH_z			
0.0635	0.0635	66,000	31.9
0.0635	0.070	62,175	28.7
0.0635	0.073	60,460	27.8
0.0635	0.076	59,250	27.2

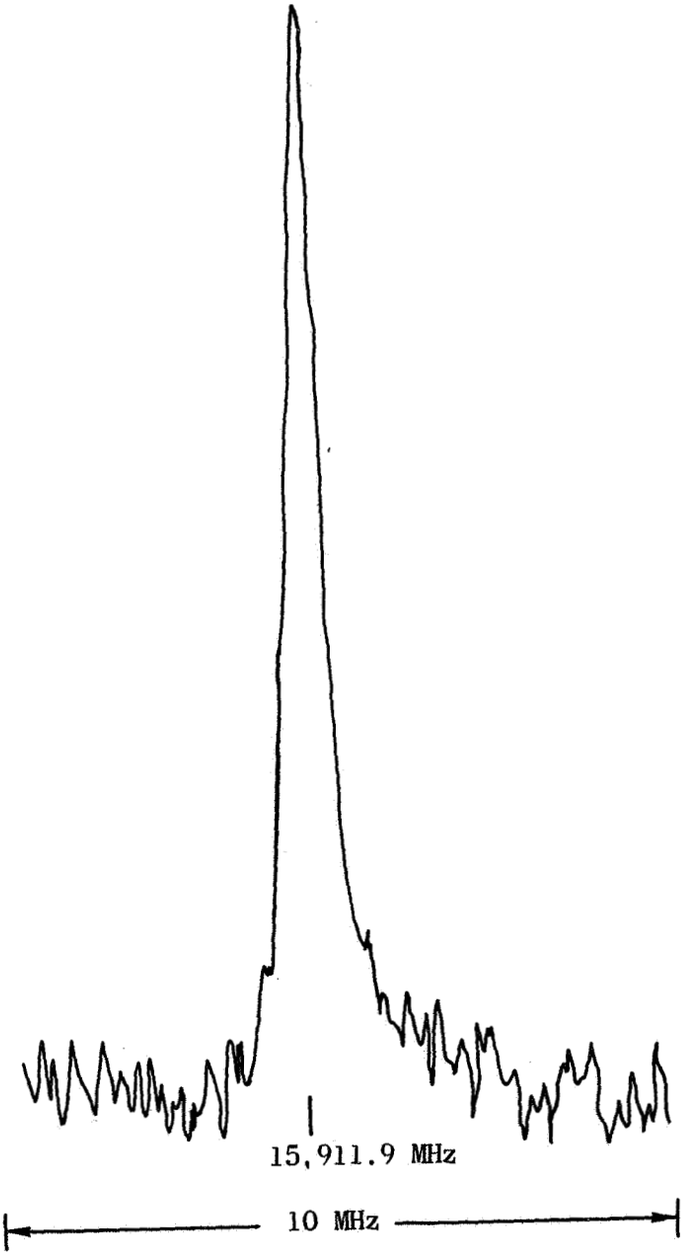

Figure 4.- Sample strip chart recording of the $0_{00} \rightarrow 1_{11}$, $1_{11} \leftarrow 2_{02}$ double resonance of methylene chloride with the modulated pump signal being slowly swept across 15,911.9 MHz.

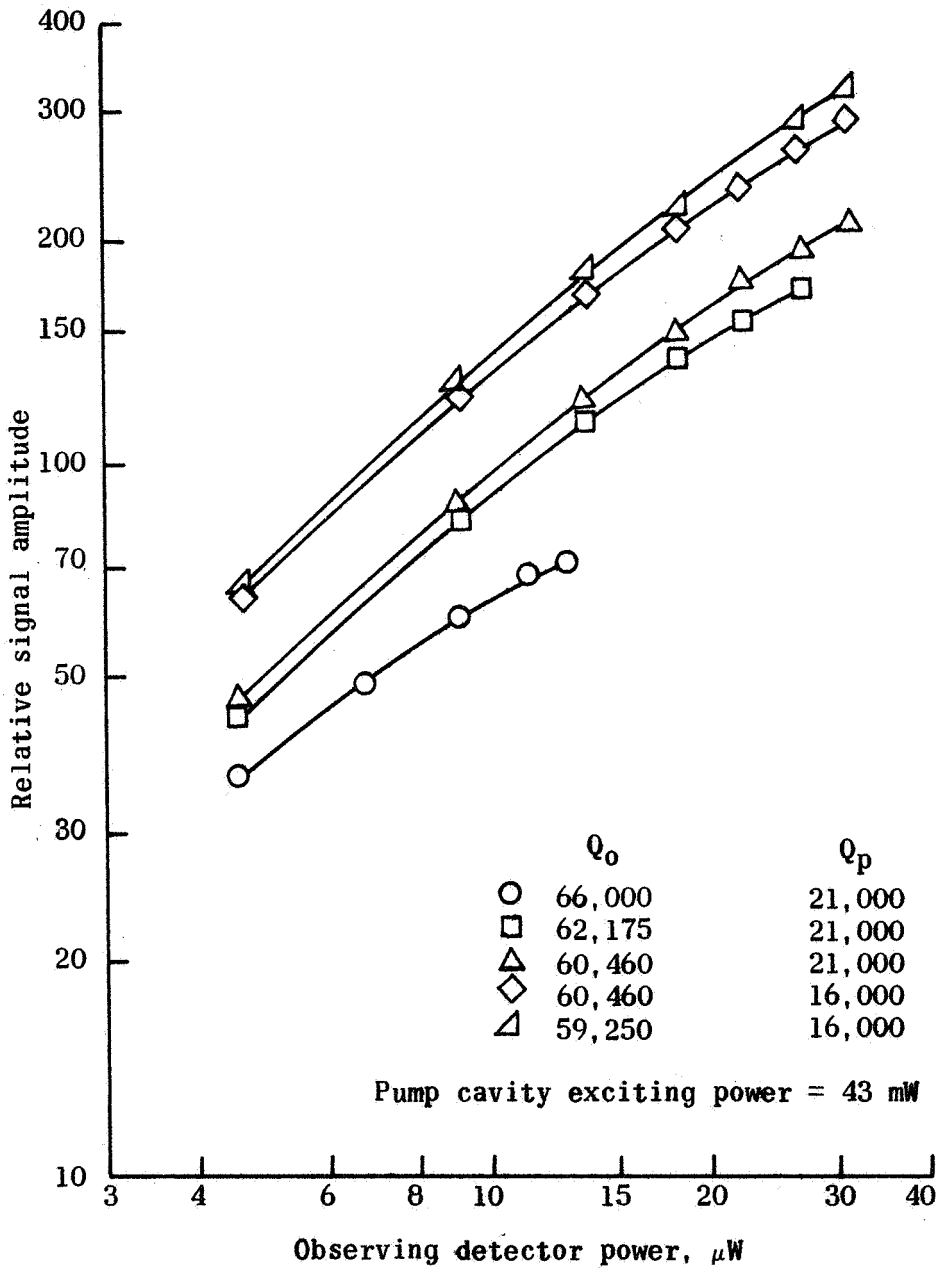

Figure 5.- Signal amplitude variations for the $0_{00} \rightarrow 1_{11}$, $1_{11} \leftarrow 2_{02}$, double resonance of methylene chloride at 100 microns pressure.

power producing more detector power. A slight decrease in Q is noted and is the result of the increased loss of energy from the cavity to the detector.

The lower three curves on Figure 5 are for constant conditions of the pump cavity and increasing observing detector iris size, hence, decreasing Q_o. Since the slopes of the curves decrease with increasing observing detector power (observing detector power is proportional to power level in the sample) it is evident that a nonlinear or saturation effect exists for this type molecular absorption effect. This effect is decreased as the ratio of observing cavity power to detector power is decreased.

Next, the power inlet iris of the pump cavity was increased and a new set of data taken for the case of $Q_o = 60, 460$. As can be seen in Figure 5, more signal was obtained for the same conditions of observing detector power. This indicates that the pump transition, $1_{11} \leftarrow 2_{02}$, was being more effectively modulated by a higher power density. For the increased power density, the observing detector iris diameter was increased again. The upper curve in Figure 5 shows the signal amplitude variation for this set of conditions.

The observing detector power is presented on the signal plots due to noise considerations. The noise in the observing circuit results primarily from the constant thermal noise of the microwave diode detector and noise resulting from external RF thermal sources. The latter output noise is proportional to the input signal power due to heterodyning of the signal with noise and due to the modulation sensitivity of the

diode (slope of the voltage-current curve). Figure 6 is a plot of noise at the recorder of the system for the same range of observing detector with no sample present in the absorption. The units of noise on Figure 6 are the same as the units of signal on the signal amplitude plots. The observing cavity Q has a negligible effect on the noise level due to the fact that the observing signal frequency is stabilized at the peak of the observing cavity response.

Figure 7 is a plot of the signal-to-noise ratio for the conditions corresponding to the upper curve of Figure 5. It is seen on this plot that an optimum signal-to-noise exists at a detector power level which is above the thermal noise limiting range.

Figures 8, 9, and 10 show the signal amplitude variations for four values of pump cavity excitations at 25, 100, and 150 microns of pressure. A pressure of 100 microns is seen to give maximum signal from the double-resonance effect for a particular set of cavity parameters.

The sensitivity of this experimental system was compared to that of an available Stark modulated spectrometer. It was found that the Stark spectrometer was a factor of approximately two more sensitive than the experimental cavity system. A more favorable comparison of the cavity system to the Stark system should result as higher frequency systems which will have inherently higher cavity Q's are investigated. More efficient modulation of a higher frequency double-resonance transition should be possible with the higher pump cavity power density available with the higher Q.

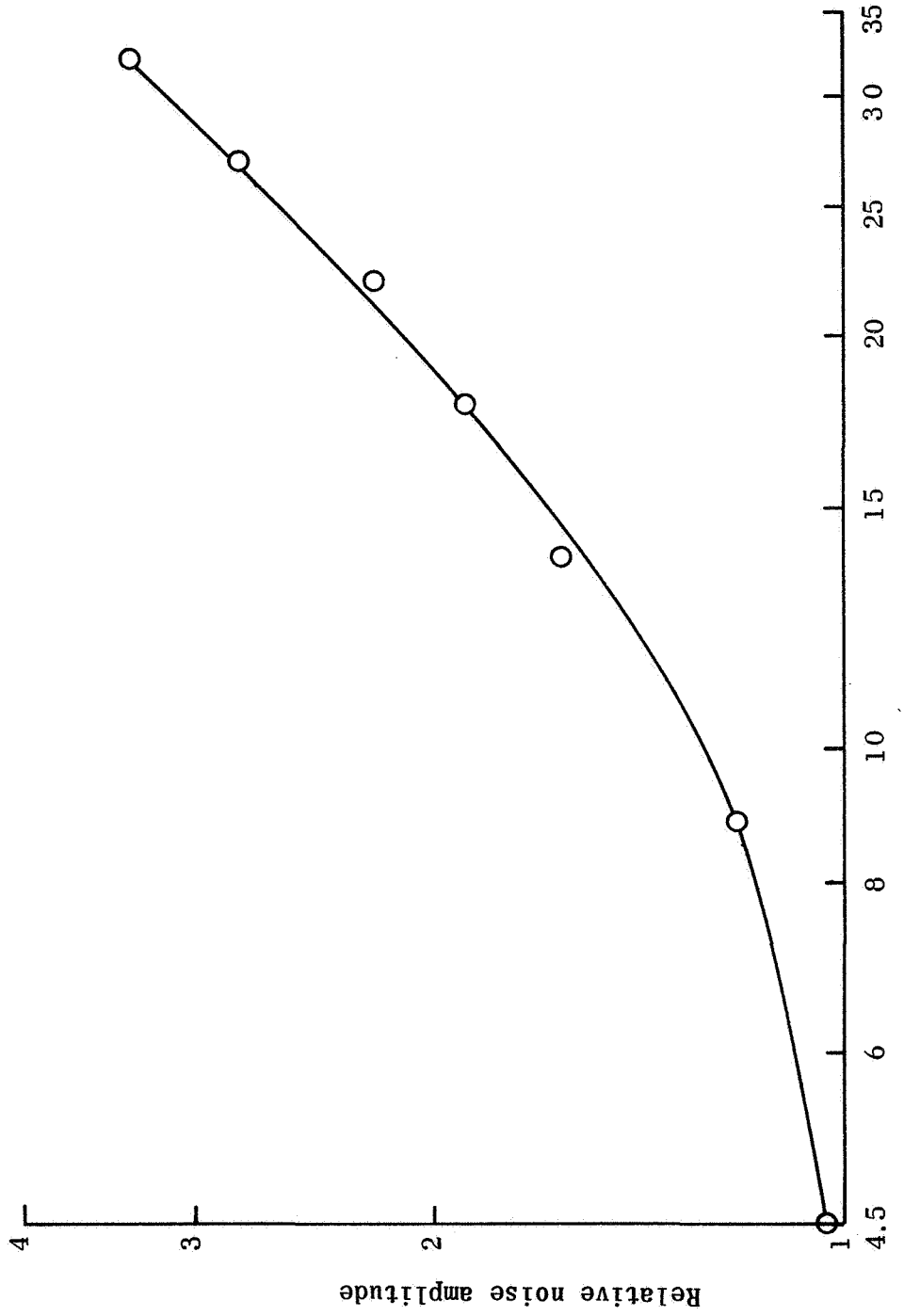

Figure 6.- Noise amplitude plot for the observing circuit.

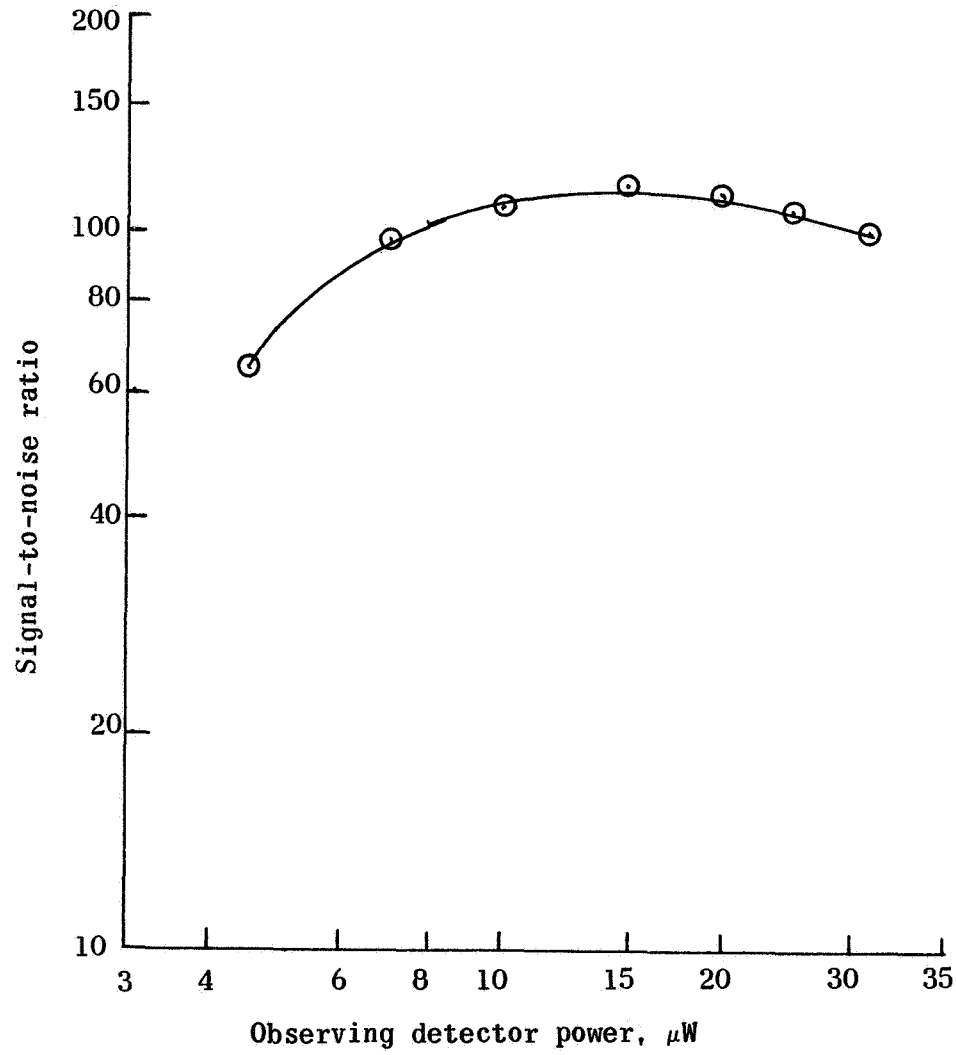

Figure 7.- Signal-to-noise ratio variation of the $0_{00} \rightarrow 1_{11}$, $1_{11} \leftarrow 2_{02}$, double resonance of methylene chloride at 100 microns pressure with Q_p = 16,000 and Q_o = 59,250.

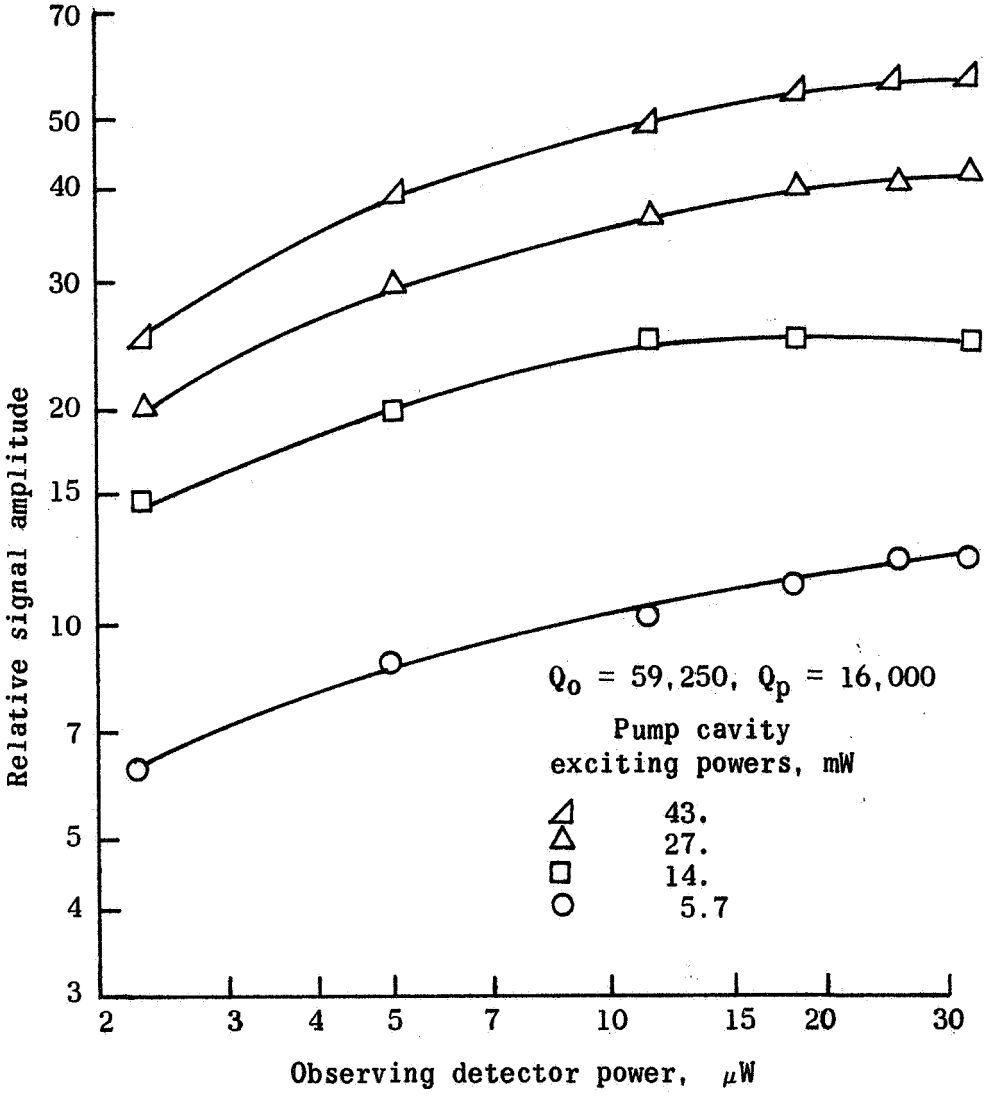

Figure 8.- Signal amplitude variations for the $0_{00} \rightarrow 1_{11}$, $1_{11} \leftarrow 2_{02}$, double resonance of methylene chloride at 25 microns pressure and different levels of pump cavity excitation power.

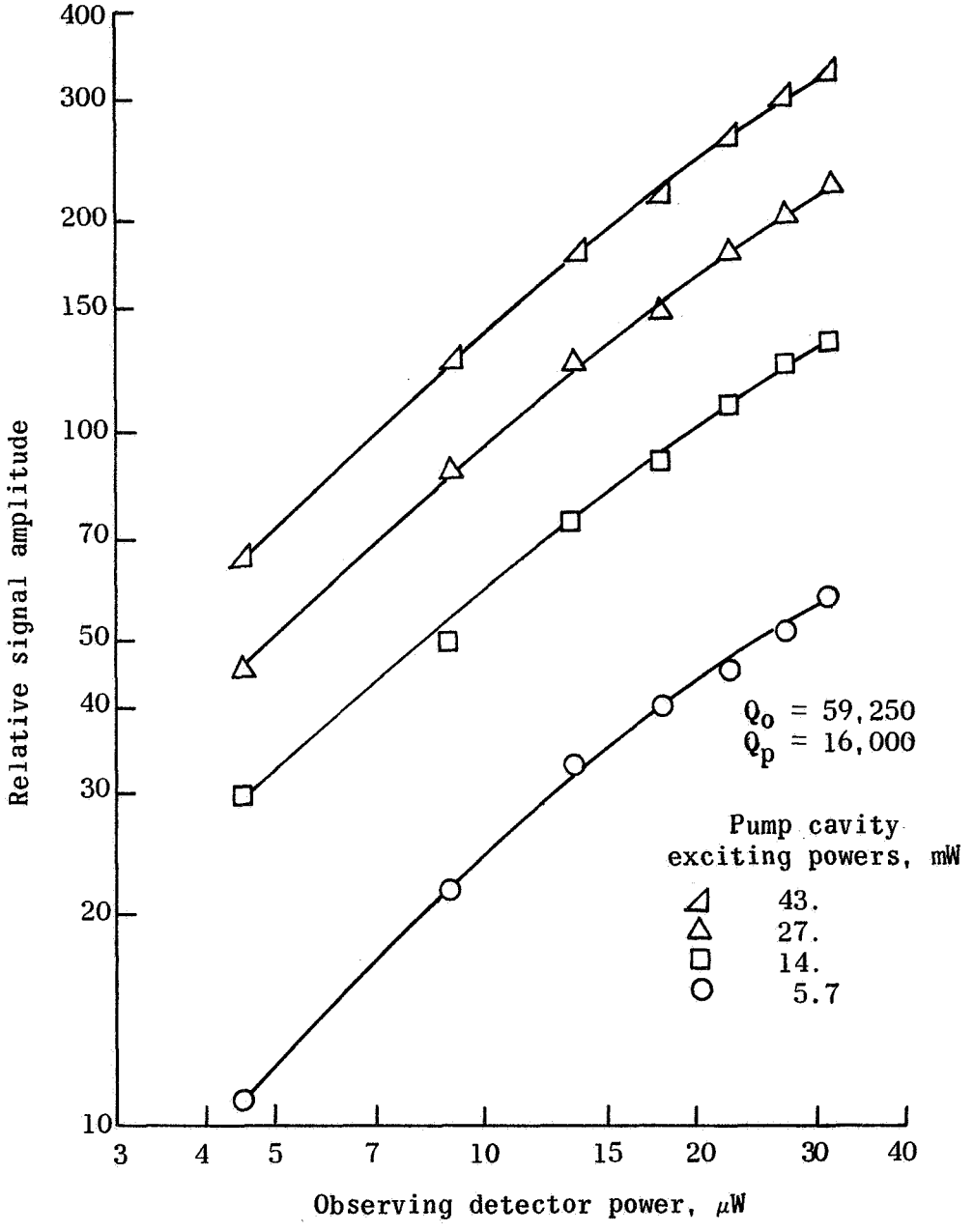

Figure 9.- Signal amplitude variations for the $0_{00} \rightarrow 1_{11}$, $1_{11} \leftarrow 2_{02}$, double resonance of methylene chloride at 100 microns pressure and different levels of pump cavity excitation power.

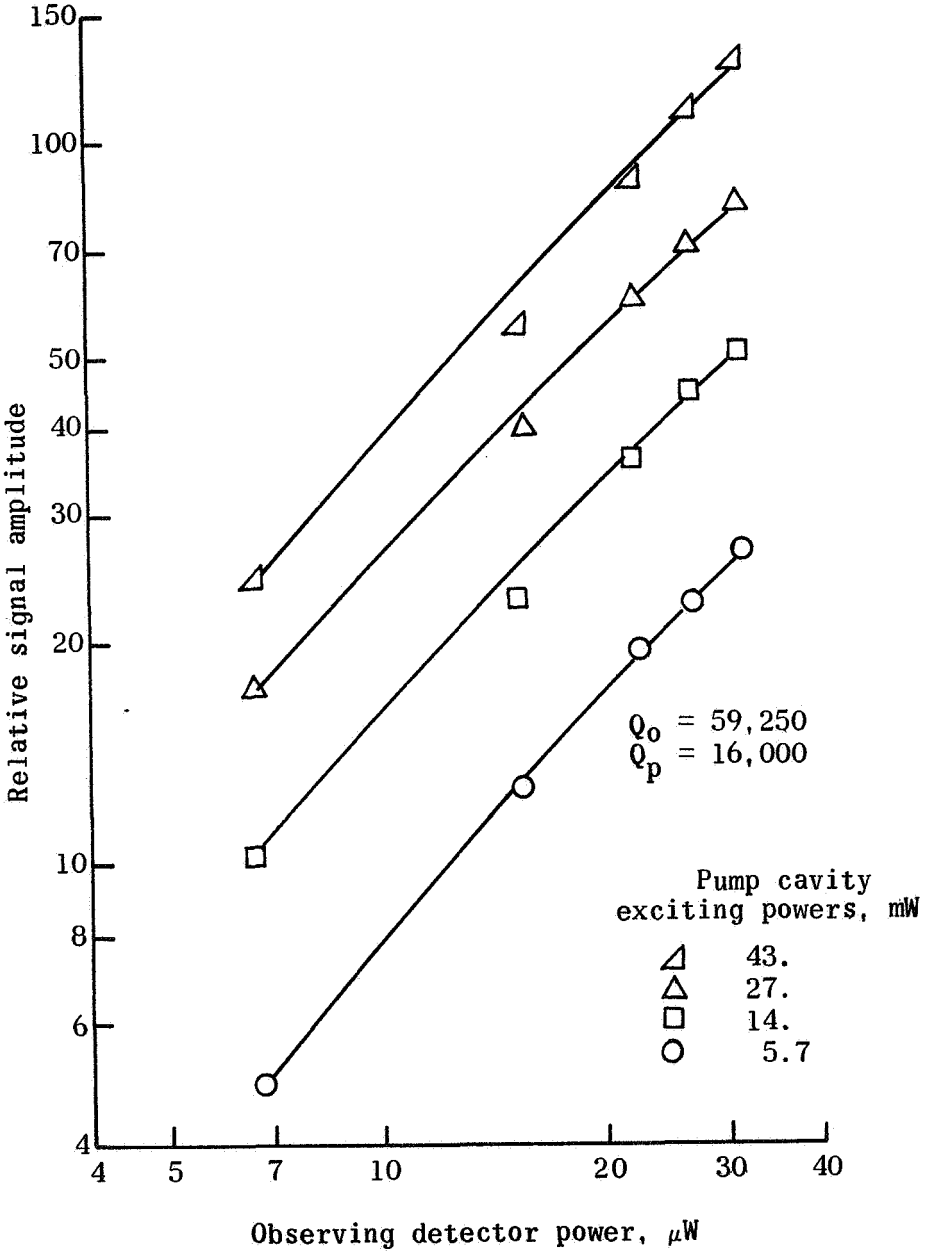

Figure 10.- Signal amplitude variations for the $0_{00} \rightarrow 1_{11}$, $1_{11} \leftarrow 2_{02}$, double resonance of methylene chloride at 150 microns pressure and different levels of pump cavity excitation power.

CHAPTER V

CONCLUSIONS

This investigation has illustrated the effectiveness of the dual resonant cavity design for use in microwave double-resonance spectroscopy.

Sensitivity Factors

For the cases studied, the factor limiting sensitivity was the amount of pump power available. Thus, with the application of higher power sources to excite the pump cavity, considerable increases in the detected signal levels should result. This increase should be approximately proportional to pump power until saturation of the pump transition occurs. Optimization of the dual resonant cavity absorption cell for the detection of a particular double-resonance transition with a given amount of cavity excitation powers is possible by varying the iris for each cavity.

Sample Properties

Improved vacuum characteristics for this absorption cell were noted as compared to the waveguide type cell. Sample equilibrium was easier to obtain. This resulted from the smaller surface to volume ratio inherent in the nearly cubical design. The orthogonal Fabry-Perot configuration results in most of the molecules of the sample being many mean free paths from a surface. This is particularly important in

obtaining a representative gas sample for the case of mixtures where differential adsorption may occur.

Frequency Capability

The physical layout of the resonant cavities provides good isolation between the pump and the observing microwave fields so that any desired combination of frequencies should be usable. Its frequency range may be extended to frequencies higher than those utilized here and even better results are anticipated because of the higher Q's which can be achieved.

REFERENCES

1. Volpicelli, R. J.; Stiefvater, O. L.; and Flynn, G. W.: "A Study of Trace Contaminant Identification By Microwave Double Resonance Spectroscopy." NASA CR-967, December 1967.

2. Townes, C. H.; and Shawlow, A. L.: "Microwave Spactroscopy." John Wiley and Sons, New York, 1953.

3. Woods, R. C., III; Ronn, A. M.; and Wilson, E. B., Jr.: "Double Resonance Modulated Microwave Spectrometer." The Review of Scientific Instruments, 37:927-933, July 1966.

4. French, I. P.; and Arnold, T. E.: "High-Q Fabry-Perot Resonator for Nitric Oxide Absorption Measurements at 150 GH_z." The Review of Scientific Instruments, 38:1604-1607, November 1967.

5. Martin Company, Orlando, Florida: "Atmospheric Absorption Measurements Using a Fabry-Perot Interferometer." Internal Paper.

6. Praddaude, H. C.: "100 KH_z Homodyne, 35 GH_z Reflection-Cavity Spectrometer With Phase-Lock of the Reference Signal and Low Frequency Field Modulation." The Review of Scientific Instruments. 38:339-347, March 1967.

7. Strauch, R. G.; Cupp, R. E.; and Gallagher, J. J.: "Quasi-Optical Techniques in Millimeter Spectroscopy." The Martin Company, Orlando, Florida.

8. Harrington, Howard W.: "On the Separation of the Broadening-Relaxation Time and Molecular Concentration from Pure-Rotational Spectroscopic Intensity Data." The Journal of Chemical Physics, 46:3698-3707, May 15, 1967.

9. Culshaw, W.: "Resonators for Millimeter and Submillimeter Wavelengths." IRE Transactions on Microwave Theory and Techniques, 9:135-144, March 1961.

10. Zimmerer, R. W.; Anderson, M. V.; Strine, G. L.; and Beers, Y.: "Millimeter Wavelength Resonant Structures." IEEE Transactions on Microwave Theory and Techniques, 11:142-149, March 1963.

11. Cox, A. P.; Flynn, G. W.; and Wilson, E. B., Jr.: "Microwave Double-Resonance Experiments." The Journal of Chemical Physics, 42:3094-3105, May 1, 1965.

12. Boyd, G. D.; and Kogelnik, H.: "Generalized Confocal Resonator Theory." The Bell System Technical Journal, 1347-1369, July 1962.

APPENDIX I

CONFOCAL FABRY-PEROT RESONANT CAVITY*

The basic confocal Fabry-Perot interferometer configuration is shown in Figure 11. Each of the mirrors is a portion of a sphere. The center of curvature of each reflector lies at the center of the conjugate reflector, that is, confocal or coincident focal points.

The modes supported by a Fabry-Perot confocal resonator are represented by TEM_{qmn} where

q = integral number of half wavelengths between reflectors

m = number of field reversals in a direction transverse to the interferometer axis of symmetry

n = number of field reversals in a transverse direction orthogonal to the direction assumed for m

When the reflectors are separated by a distance, b, equal to their common radii of curvature, the condition for resonance is given by

$$\frac{4b}{\lambda} = 2q + (1 + m + n) \qquad \text{(I-1)}$$

When the spherical reflectors are separated by a distance, d, which is not equal to the radius of curvature of the reflectors, the conditions for resonance are given by

$$\frac{4d}{\lambda} = 2q + (1 + m + n)\left[1 - \frac{4}{\pi} \tan^{-1} \frac{b - d}{b + d}\right] \qquad \text{(I-2)}$$

---

*Reference 4.

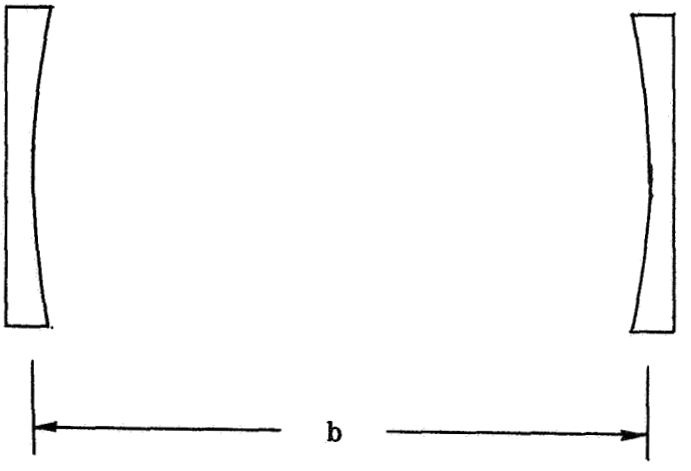

Figure 11.- Confocal interferometer configuration.

For the dominant mode, $m = n = 0$, the conditions for resonance reduce to

$$\frac{4b}{\lambda} = 2q + 1 \tag{I-3}$$

and

$$\frac{4d}{\lambda} = 2q + \left[1 - \frac{4}{\pi} \tan^{-1} \frac{b - d}{b + d}\right] \tag{I-4}$$

for the confocal and nonconfocal cases, respectively.

A semiconfocal system makes use of the symmetry of the interferometer by placing a flat mirror at the midpoint between the confocal spherical mirrors as shown in Figure 12. The advantage of this configuration is the ease with which energy can be coupled into and out of the resonator by small irises. The same conditions of resonance apply (eqs. (I-3) and (I-4)) where b is the confocal radius of curvature. Resonance in the semiconfocal case can only occur when q is an even integer because of the boundary condition requiring the electric vector to be zero at the metallic surface of the flat mirror.

For a closely coupled resonator the ratio of the electric field within the cavity, E_c, to the electric field, E_t, in the transmission line driving it is approximately (Ref. 7, p. 590)

$$\frac{E_c}{E_t} = \left(\frac{QA_o}{A_r q\pi}\right)^{1/2} \tag{I-5}$$

where A_r and A_o are the effective areas of the resonator and input transmission line, respectively. For the observing cavity of this

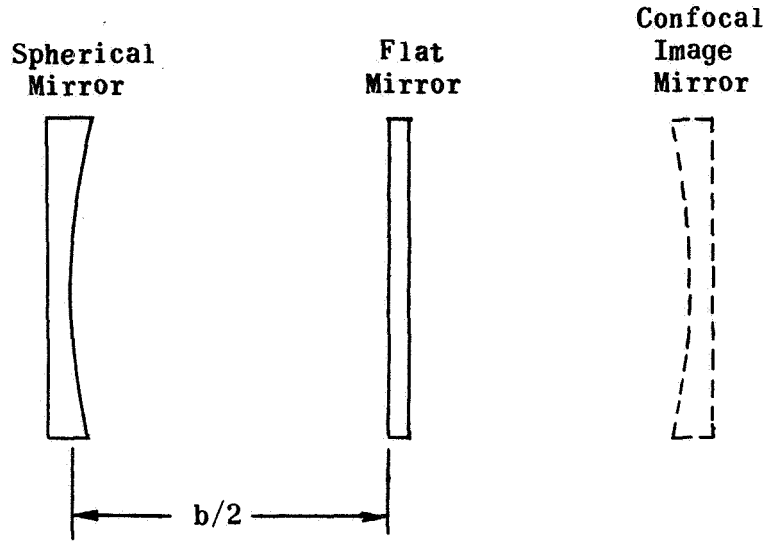

Figure 12.- Semiconfocal interferometer configuration.

experiment A_r and A_o are constant since the inlet iris diameter was held constant while the outlet iris diameter was varied (see Table I). The quantity q is a positive integer defined as

$$q = \frac{b}{\lambda} \tag{I-6}$$

For the observing cavity of this experiment

$$\frac{E_c}{E_t} = CQ^{1/2} \tag{I-7}$$

where C is a constant. Furthermore, if E_t is held constant, then

$$E_c = C_1 Q^{1/2} \tag{I-8}$$

Since the power inside the cavity, P_c, varies as E_c^2 then

$$P_c = C_2 Q \tag{I-9}$$